# Citrate sol-gel synthesis of $BaAl_2O_4$:x% $Cu^{2+}$ ($0 \leq x \leq 1$) nano-phosphors: structural, morphological and photoluminescence properties

**V.M. Maphiri[1], M.R. Mhlongo[1], T.T. Hlatshwayo[2], T.E. Motaung[3], L.F. Koao[4], S.V. Motloung[1,5*]**

[1]Department of Physics, Sefako Makgatho Health Science University, P. O. Box 94, Medunsa, 0204, South Africa

[2]Department of Physics, University of Pretoria, Pretoria, 0002, South Africa

[3]Department of Chemistry, University of Zululand, KwaDlangezwa 3886, South Africa

[4]Department of Physics, University of the Free State, Qwaqwa Campus, Private Bag X13, Phuthaditjhaba 9866, South Africa

[5]Department of Physics, Nelson Mandela University, P. O. Box 77000, Port Elizabeth 6031, South Africa

Corresponding author:

E-mail: cchataa@gmail.com (Setumo Victor Motloung)

## Highlights

- Hexagonal nanocrystalline $BaAl_2O_4$:x% $Cu^{2+}$ ($0 \leq x \leq 1$) phosphor powders were succesfully prepared via the citrate sol-gel technique.
- Photoluminescence emission intensity of the powder sample was dependent on the $Cu^{2+}$ concentration.
- Both emissions from the host and $Cu^{2+}$ were observed.
- The Commission on Illumination color coordinate evidently showed that the bluish emission depends on the $Cu^{2+}$ concentration.
- Themoluminescence results showed the precence of both the shallow and deep level tranps in $BaAl_2O_4$: $Cu^{2+}$ phosphor material.

## Abstract

This paper reports on the effects of varying the $Cu^{2+}$ doping concentration on the structure, morphology and optical properties of the $BaAl_2O_4$ phosphor. $BaAl_2O_4$:x% $Cu^{2+}$ ($0 \leq x \leq 1$) series were successfully synthesized via citrate sol-gel method. The X-ray diffraction (XRD) results revealed that the prepared phosphor sample consist of a single phase hexagonal structure. The presence of Ba, Al, O and Cu were confirmed by the energy dispersive X-ray spectroscopy (EDS). Scanning electron microscope

(SEM) revealed that the morphology of the prepared samples highly depends on the $Cu^{2+}$ concentration. Transmission electron microscopy (TEM) results revealed the hollow tubular and nano-nature of the crystallite sizes. When the un-doped sample was excited at 283 nm, the photoluminescence (PL) results revealed six emission peaks located at 420, 435, 457, 521, 612 and 722 nm, which were attributed to the intrinsic intra band gap defects within the $BaAl_2O_4$ (host). The emission at 425 nm observed for the $BaAl_2O_4$:$Cu^{2+}$ samples was attributed to the $3d^84s^1 \rightarrow 3d^9$ transition in $Cu^{2+}$ ion. The optimum doping $Cu^{2+}$ concentration was found to be 0.075% $Cu^{2+}$. Critical energy transfer distance ($R_c$) of $Cu^{2+}$ ions was found to be 12.01 Å, which suggested that the multipole-multipole interaction was the main reason for the luminescence quenching. The International Commission on Illumination (CIE) colour showed that the bluish emission colour of the prepared samples depends on the excitation wavelength and $Cu^{2+}$ concentration. Thermo stimulated luminescence (TSL) of the host material showed the presence of both the swallow and deep traps respectively located at 75 and 240 °C.

**Keywords:** Citrate sol-gel; $Cu^{2+}$-doped; Luminescence; CIE

## 1. Introduction

Long afterglow phosphor materials such as barium aluminates ($BaAl_2O_4$) have attracted many researchers around the globe due to their potential in light emitting devices [1,2]. The afterglow property is normally observed when this material is doped with foreign ions [1]. The most common rare earth (RE) ions investigated by many researchers are the $Eu^{2+/3+}$ and $Dy^{3+}$ [1,2]. Rezende et al. [1] reported the computational and experimental comparative study of the optical properties of the $BaAl_2O_4$:$Eu^{3+}$. Both the computational and experimental results showed that $Eu^{3+}$ preferentially substitute the $Ba^{2+}$. The PL emission of $BaAl_2O_4$:$Eu^{3+}$ showed the presence of several narrow emission peaks that ranged from 550 – 750 nm, which were attributed to the forbidden electric-dipole 4f → 4f ($^5D_0 \rightarrow {}^7F_J$, J = 0 – 4) transitions within the $Eu^{3+}$ ion. Not only $BaAl_2O_4$ have been doped with $Eu^{3+}$ ion, divalent europium ($Eu^{2+}$) ion [2,3] and several other RE ions such as trivalent neodymium ($Nd^{3+}$) [3], dysprosium ($Dy^{3+}$) [4] and cerium ($Ce^{3+}$) [5] have been used as dopants into the $BaAl_2O_4$ system. These sol-gel method have been found to be an effective and attractive techniques for the synthesis of nanoparticle phosphor materials [7]. However, there are scarce reports on the fabrication of $BaAl_2O_4$ nanoparticles via citrate sol-gel method, on the other hand the transition metal such as copper (Cu), which is known for the excellent electric and thermal properties has never been reported as a possible dopant into the $BaAl_2O_4$ system. Previous studies have shown the possible and successful incorporation of $Cu^{2+}$ into metal oxides such as ZnO [6] and

$ZnAl_2O_4$ [7]. Koao et al. [6] showed that the reflectance intensity decreased with an increase in the molar concentration of $Cu^{2+}$ in ZnO. There was no observed shift on the absorption band and the ZnO sample was found to have the highest luminescence intensity, while the addition of $Cu^{2+}$ resulted in luminescence quenching. Motloung et al. [7] reported the sol-gel synthesis of the $ZnAl_2O_4$:x% $Cu^{2+}$ ($0 \leq x \leq 1.25$) system. The reflectance intensity of the 270 nm was observed to vanish as the concentration of $Cu^{2+}$ was increased. The PL showed the presence of three emission peaks at 394, 405 and 574 nm. The peak at 394 nm was credited to the common intrinsic intraband gap defects. Emission peaks observed at 405 and 574 nm were attributed to the $Cu^{2+}$ transitions particularly from the excited state $3d^84s^1 \rightarrow 3d^9$ (ground state). The same luminescence quenching observed in Koao et al. [6] when doping with $Cu^{2+}$ was also observed. Our previous study [7], proposed and recommended for further investigations on the x% $Cu^{2+}$ concentration for the window region $x < 0.125\%$ in order to explore the optimum $Cu^{2+}$ concentration. With this mentality, the current study is basically driven by the desire to explore $Cu^{2+}$ optimum concentration in $BaAl_2O_4$ with the main objective of producing new and alternative oxide phosphor for blue light emitting diodes (BLEDs). This report investigates the effect of varying $Cu^{2+}$ concentration on the structure and optical properties of the $BaAl_2O_4$:x% $Cu^{2+}$ ($0 \leq x \leq 1$) nano-phosphors prepared using the citrate sol-gel method. The optimum concentration was found to be 0.07% $Cu^{2+}$. The associated excitation and emission channels are also proposed.

## 2. Experimental

### 2.1. Sample synthesis

A series of the $BaAl_2O_4$:x% $Cu^{2+}$ ($0 \leq x \leq 1$) nano-phosphors were synthesized via citrate sol-gel technique. The host or un-doped $BaAl_2O_4$ was prepared by dissolving 3.881 g of barium nitrates [$Ba(NO_3)_2$, 99%], 10.919 g of aluminium nitrates nano-hydrate [$Al(NO_3)_3 \cdot 9H_2O$, 99%] and 2.328 g of citric acid (CA) [$C_6H_8O_7 \cdot H_2O$, 99%] in deionized water. Specified amounts of copper nitrate tri-hydrate [$Cu(NO_3)_2 \cdot 3H_2O$, 98%] were added to dope $BaAl_2O_4$ with x% $Cu^{2+}$ ($0 \leq x \leq 1$). The chemicals or reagents used in this study were purchased from Sigma Aldrich and they were used without any further purification. For all samples, the heating temperature on the magnetic stirrer was kept at ~ 80 °C, while constantly stirring the solution until the gels were formed. The gels were then left to dry at room temperature for 12 h in order to allow more and enough gelling. Afterwards, the prepared gels were then annealed at 1000 °C in a furnace for 2 h. The annealed gels were then crashed using mortar and pestle for fabrication of the powder samples and they were then taken for analysis and characterization with different techniques.

### 2.2. Characterization

The structure and crystallite sizes of the prepared nano-powders were studied using the Bruker D8-Advance powder XRD with a CuKα (λ = 1.5405 Å) radiation. Zeiss Supra 55 electron microscope (SEM) coupled with Oxford XMax$^N$ energy dispersive X-ray spectroscopy (EDS) was used to study the surface morphology, elementary composition and distribution. Transmission electron microscopy (TEM) was performed with a JEOL JEM 1010 to study the size and shape of powder samples. Photoluminescence spectra measurements were performed at room temperature by the Hitachi F-7000 fluorescence spectrophotometer. The types of traps in the prepared material were performed using the thermo luminescence (TL) spectroscopy (Nucleonix 1009I TL reader).

## 3. Results and discussion

### 3.1 X-ray diffraction (XRD)

The XRD results are of the $BaAl_2O_4$:x% $Cu^{2+}$ ($0 \leq x \leq 1$) series are shown in Fig. 1. The prepared materials are crystalline and the diffraction peaks indicate the presence of the hexagonal single phases of $BaAl_2O_4$, which could be indexed to the JCDPS 82-2001 standard. The average lattice parameters calculated from the most prominent peaks (202) and (220) diffraction peaks were found to be $a$ = 1.035 Å and $c$ = 0.870 Å, which are corresponding to the values reported by Wako et al. [3] report. No change in the crystal structure suggests that $Cu^{2+}$ ions have been successful incorporated into $BaAl_2O_4$ crystal lattice via substitution.

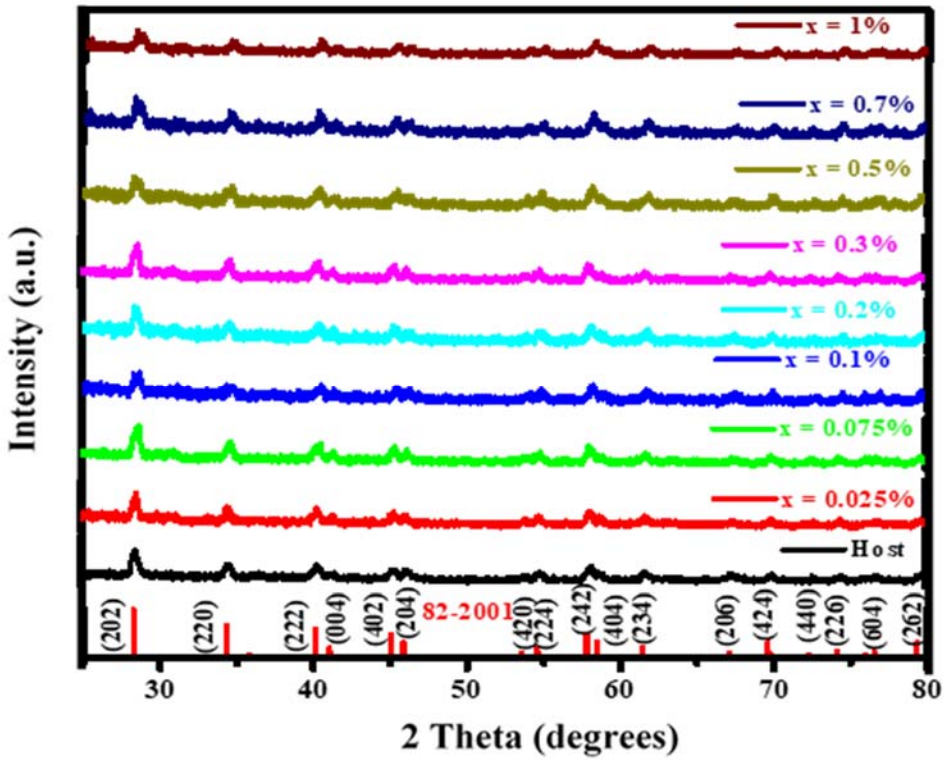


**Fig. 1.** The XRD patterns for $BaAl_2O_4$:x% $Cu^{2+}$ ($0 \leq x \leq 1$) series.

The crystallite sizes of the $BaAl_2O_4$:x% $Cu^{2+}$ ($0 \leq x \leq 1$) series was estimated particularly from the prominent diffraction peak (202) by using the Scherrer's equation (1) [8]:

$$D = \frac{0.9\lambda}{\beta \cos\theta} \qquad \ldots (1)$$

where $D$ is the crystallite size (nm), $\lambda$ is the radiation wavelength (0.15406 nm), $\beta$ is the full width at half maximum (FWHM) (in radians) and $\theta$ is the angle of diffraction (degrees). The estimated values are presented in Table 1. Varying the $Cu^{2+}$ concentration in $BaAl_2O_4$:x% $Cu^{2+}$ influenced the crystallites sizes although there are fluctuations. Thus, the crystallite sizes depends on the $Cu^{2+}$ concentration.

**Table 1.** Sample identification and crystallites size.

| Sample ID | Crystallite size (nm) |
|---|---|
| Host | 20 |
| x = 0.025% | 24 |
| x = 0.075% | 17 |
| x = 0.1% | 22 |
| x = 0.2% | 23 |
| x = 0.3% | 20 |
| x = 0.5% | 17 |
| x = 0.75% | 16 |
| x = 1.0% | 19 |

### 3.2 Energy dispersive X-ray spectroscopy (EDS)

The EDS technique was employed to confirm the elementary composition of the selected prepared nano-powders as shown in Fig. 2. The results confirmed that the expected elements Ba, Al, O and Cu for the host (Fig. 2 (a)) and $Cu^{2+}$ doped (Fig. 2 (b)) samples, respectively. In both spectra, the carbon (C) signal or peak is attributed to the carbon tape used to coat the sample in a preparation prior to EDS measurement. There was no evidence of any extra peaks which could be related to the impurities and this is in agreement with the XRD results presented in Fig. 1.

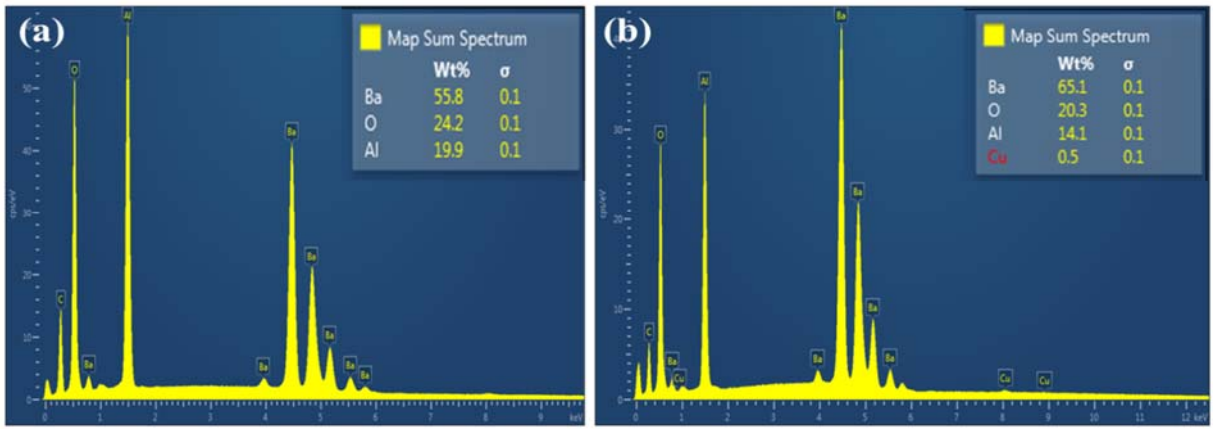


**Fig. 2.** The EDS spectrum for the (a) x = 0 (host) and (b) 1.0% $Cu^{2+}$ samples.

EDS mapping was performed on the x = 1.0% sample and the images are illustrated in Fig. 3. The images of individual elements are displayed around the layered image. The images reveal that the compositional elements of the phosphor are distributed homogenously all over its surface such results are similar to those reported by our group [8]. On the contrary, elements might heterogeneously clump together [9].

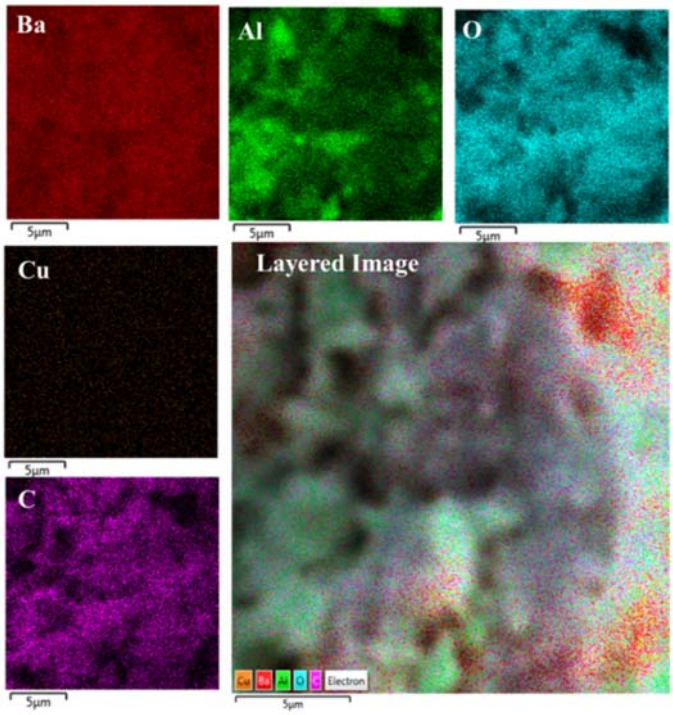


**Fig. 3.** EDS mapping image of the $BaAl_2O_4$:1.0% $Cu^{2+}$.

### 3.3 Scanning electron microscope (SEM)

The morphology of the selected nano-phosphor was analyzed by the SEM as shown in Fig. 4. The host micrograph in Fig. 4 (a) consists of the irregular particles with very clear sharp corners and in some instances, the hexagonal shape (indicated by the red arrow) structures are observed. These hexagonal structures are certainly attributed to $BaAl_2O_4$ particles as suggested by the XRD results in Fig. 1. The nature of some of these hexagonal structures seems to be hollow and tubular as indicated by the red arrow in Fig. 4 (a). For the x = 0.025% shown in Fig. 4 (b), the micrograph shows more or higher degree of the hexagonal particles with shorter rods-like structures. As the $Cu^{2+}$ concentration was increased to x = 1.0% (see Fig. 4(c)), the morphology clearly change to the elongated hexagonal rods structures attached to each other. The results suggest that the morphology of the prepared $BaAl_2O_4$:x% $Cu^{2+}$ nano-phosphor depends on the $Cu^{2+}$ concentration. Koao et al. [6] observed similar kind of behavior when the $Cu^{2+}$ ions were

varied in ZnO system. The flower-like structure was observed to change to a mixed structure with the emergence of irregular shapes with an increase in $Cu^{2+}$ concentartion.

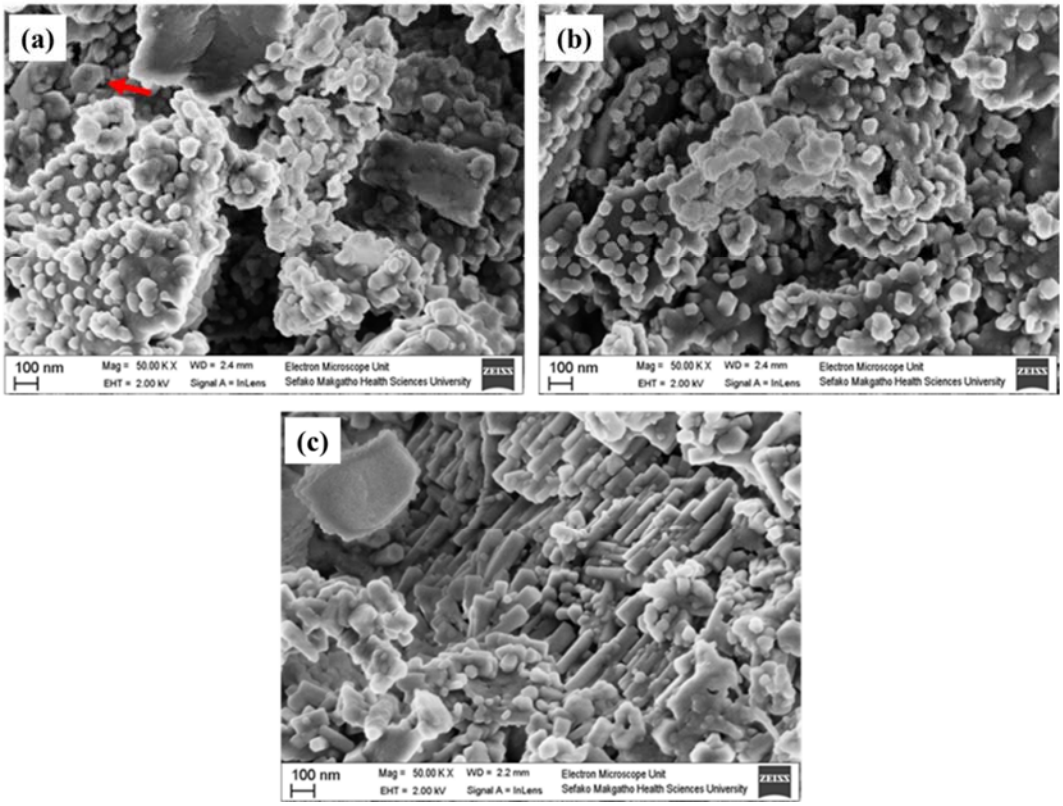


**Fig. 4.** SEM photographs for the (a) host, (b) x = 0.025 and (c) 1.0% $Cu^{2+}$ doped nano-powders.

### 3.4 Transmission electron microscopy (TEM)

The TEM image of the host and x = 1.0% are respectively shown in Fig. 5 (a) and (b). The results revealed that the host sample also consists of the hollow tubular rods structures. For the x = 1.0%, the results confirms the agglomerated rods-like-needle structures, which are attached to each other. The average crystallite sizes of the host sample on the cross sectional areas seems to be around 20 nm. It is very clear that the XRD, SEM and TEM complement each other.

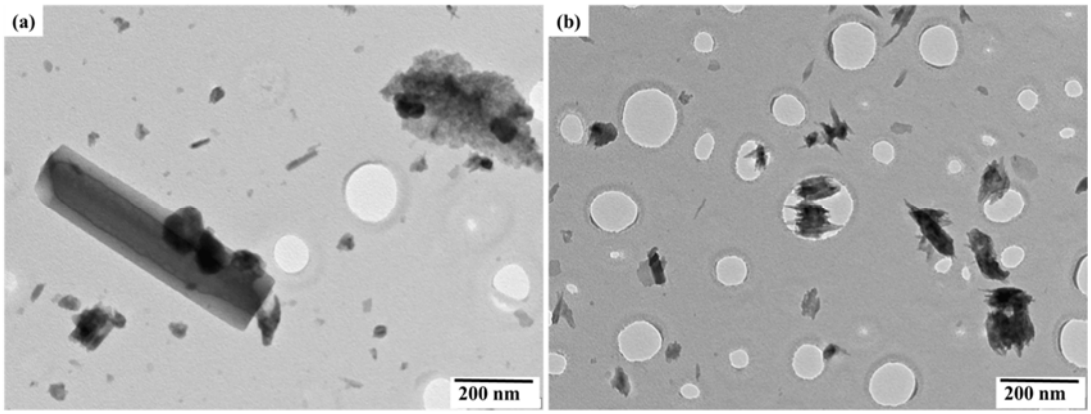


**Fig. 5.** TEM images of the (a) host and (b) x = 1.0% $Cu^{2+}$ doped samples.

### 3.5 Photoluminescence (PL) spectroscopy

The room temperature PL excitation and emission spectra of the $BaAl_2O_4$:x% $Cu^{2+}$ ($0 \leq x \leq 1$) series are shown in Fig. 6 (a). When monitoring an emission at 435 nm, the excitation spectra indicates the presences of two absorption bands located at 225 and 283 nm. These absorption bands are attributed to the band-to-band transition and defects absorption in $BaAl_2O_4$, respectively [10]. When monitoring the excitation at 283 nm, the emission spectra revealed an emission band located at 424 – 475 nm. In order to trace all of the emissions arising from the host material, the deconvolution emission spectra of the host is presented in Fig. 6 (b). The results revealed that there are distinct emissions peaks located at 420, 435, 457, 521, 612 and 722 nm. All of these emissions are certainly attributed to arise from the intrinsic defects within the host material such as oxygen vacancies ($V_O^*$). These results suggest that there are many distinct luminescence active traps located at different energy levels within the host materials. However, for the $Cu^{2+}$ doped sample, it is noted that the emission is located at 425 nm, which is attributed to the $Cu^{2+}$ from $3d^8 4s^1 \rightarrow 3d^9$ transition [7,9]. However, it is emphasized that the contribution from the host material cannot be ignored. Emission intensity as a function of the $Cu^{2+}$ concentration is shown in Fig. 6 (c) and the results revealed the Gaussian behavior with an optimum $Cu^{2+}$ concentration at 0.07% $Cu^{2+}$. These results are clearly different from what have been observed on the previous studies in ZnO [6] and $ZnAl_2O_4$ systems [7] as $Cu^{2+}$ doping resulted in luminescence quenching in both studies. Hence, it is with this reason why the current results are very important and unique as far as the $Cu^{2+}$ doping optimization in oxide host materials is concern. Knowing the optimum, and as per Blasse formula [11,12], the critical distance ($R_C$) between the $Cu^{2+}$ activator ions can be directly calculated by the equation

$$R_C = 2\left[\frac{3V}{4\pi cN}\right]^{\frac{1}{3}} \quad \ldots (2)$$

where V is the unit cell volume, c is the optimum concentration of the activator ion and N is the number of ions present in the unit cell. Taking the N = 6, c = 0.075% $Cu^{2+}$ and V = 830.75 $Å^2$ the $R_C$ value was found to be 12.01 Å. In this study, the $R_C$ > 5 Å and this indicates that the multipole-multipole interaction is responsible for the concentration quenching [11,12]. The excitation and emission pathway channels are presented in Fig. 7. The star (*) indicates the non-radiative relaxation.

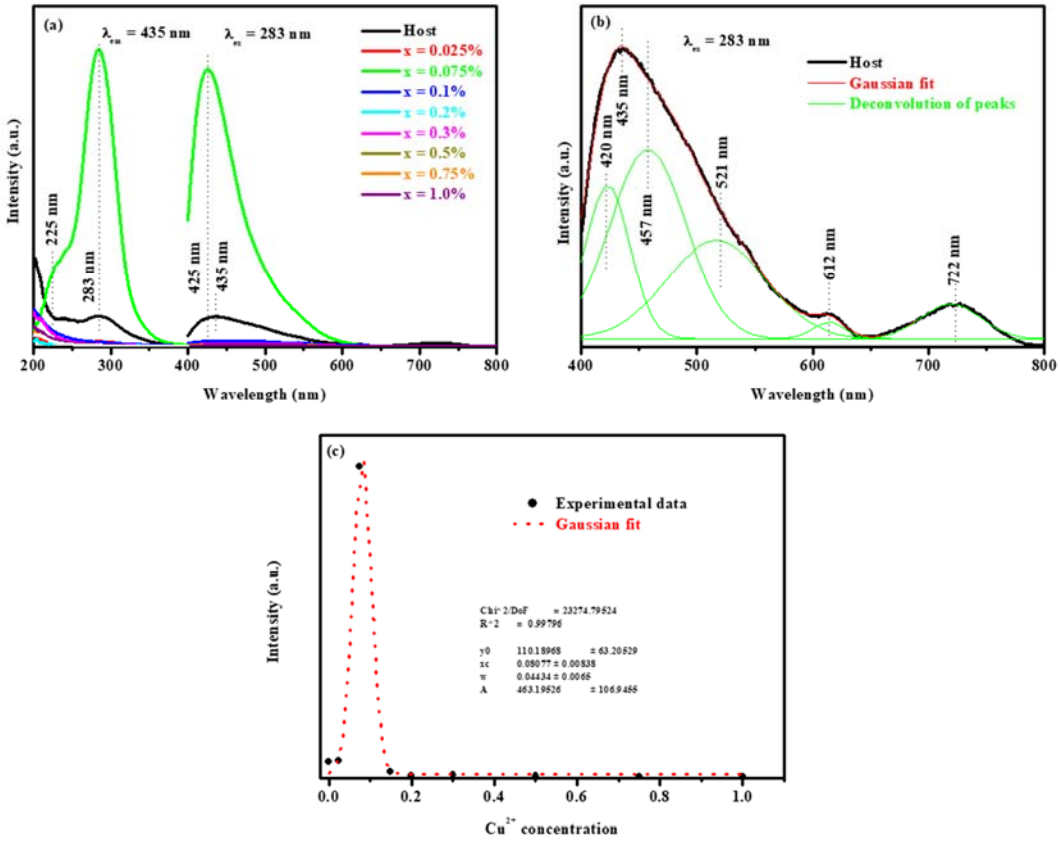


**Fig. 6.** The excitation and emission spectra of the (a) $BaAl_2O_4$:x% $Cu^{2+}$ ($0 \leq x \leq 1$) series (b) deconvolution of the host and (c) emission intensity as a function of $Cu^{2+}$ concentration.

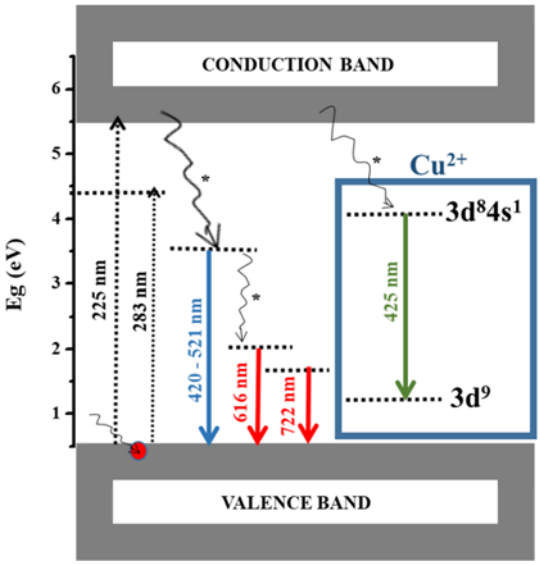


**Fig. 7.** The proposed excitation and emission pathways channel in $BaAl_2O_4$: x% $Cu^{2+}$ ($0 \leq x \leq 1$) nano-powder.

The optimum luminescence intensity x = 0.075% $Cu^{2+}$ doped sample was further excited at various excitation wavelength and the emission spectra is illustrated in Fig. 8 (a). The results revealed that the emission violet emission intensity and the peak position depends on the excitation wavelength. The emission intensity as a function of the excitation wavelength revealed the Gaussian behavior with a maximum at 283 nm, which correspond to the excitation wavelength used in Fig. 6.

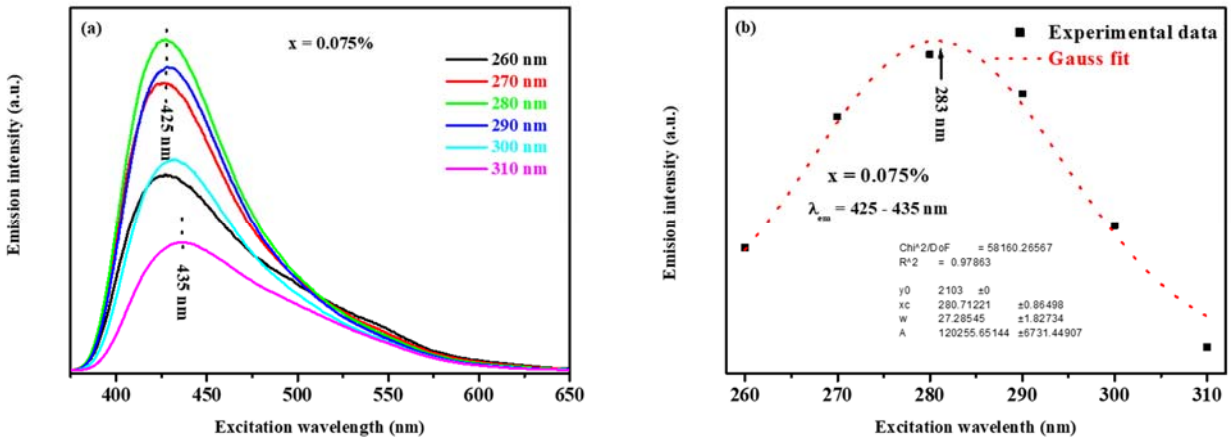


**Fig. 8.** (a) The emission spectra of the x = 0.075% excited at various excitation wavelength and (b) emission intensity as a function of excitation wavelength.

Phosphorescence lifetime of the prepared $BaAl_2O_4$: x% $Cu^{2+}$ ($0 \leq x \leq 1$) nano-phosphor excited at 283 nm when monitoring the 435 nm emission is presented in Fig. 9. All of the decay curves were fitted by the first order exponential function [13]:

$$I = A + I_0 e^{(-t/\tau)} \quad \ldots (3)$$

where $A$ is the fitting parameter, $I$ and $I_0$ are respectively the luminescence intensities at times $t$ and 0, $t$ is the time and $\tau$ is the luminescence lifetime. The lifetime values are presented in Table 2. The results showed that the photoluminescence depends on the $Cu^{2+}$ concentration.

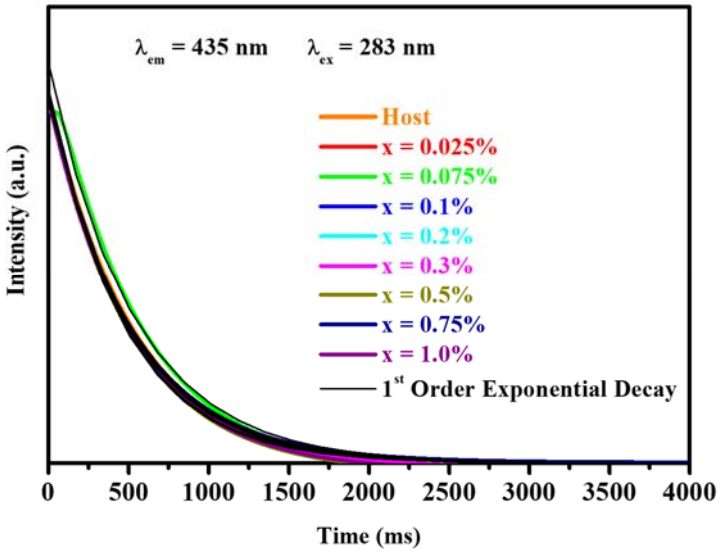


**Fig. 9.** The decay curve of the $BaAl_2O_4$: x% $Cu^{2+}$ ($0 \leq x \leq 1$) nano-powder series.

**Table 2.** Sample identification, crystallites size and CIE colour co-ordinates.

| | Lifetime | | |
|---|---|---|---|
| **Sample ID** | A | time (ms) | **CIE (x;y)** |
| Host | 10646.8 ± 35.2 | 503.0 ± 2.4 | (0.179 ; 0.189) |
| x = 0.025% | 10593.0 ± 40.0 | 479.7 ± 2.6 | (0.173 ; 0.232) |
| x = 0.075% | 11390.0 ± 31.6 | 530.3 ± 2.1 | (0.168 ; 0.243) |
| x = 0.1% | 10505.9 ± 26.0 | 496.5 ± 1.7 | (0.212 ; 0.259) |
| x = 0.2% | 10497.1 ± 26.2 | 497.3 ± 1.8 | (0.209 ; 0.273) |
| x = 0.3% | 10602.9 ± 47.6 | 472.1 ± 3.0 | (0.212 ; 0.286) |
| x = 0.5% | 10339.4 ± 3.5 | 521.8 ± 0.3 | (0.216 ; 0.294) |
| x = 0.75% | 10570.1 ± 40.7 | 478.6 ± 2.6 | (0.209 ; 0.270) |
| x = 1.0% | 10578.7 ± 44.1 | 475.4 ± 2.8 | (0.159 ; 0.272) |

The International Commission on Illumination (CIE) colour chromaticity coordinates of the prepared powders is shown in Fig. 10. The (x;y) values were calculated using the CIE coordinate calculator software [14] and the obtained values are presented in Table 2. The results showed that the $Cu^{2+}$ concentration and excitation wavelength influences the bluish emission colour.

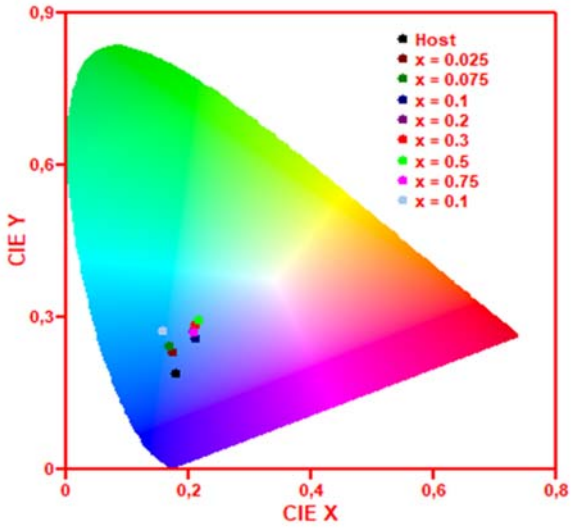


**Fig. 10.** The CEI colour of the $BaAl_2O_4$:x% $Cu^{2+}$ ($0 \leq x \leq 1$) series.

### 3.6 Thermo stimulated luminescence (TSL)

The kind of the defects on the prepared phosphor materials were analyzed by the TSL spectroscopy as shown in Fig. 11. The results revealed that the nature of the TSL glow curves for all samples are exhibits the behavior with two peaks at 75 and 240 °C. This clearly suggest that there are shallow and deep traps present in $BaAl_2O_4$:x% $Cu^{2+}$ system [15,16]. These results suggest that all of the traps originate from the host material. Based on the PL results in Fig. 7 and 8, it is clear that these traps are luminescence active and the trap density depends on the $Cu^{2+}$ concentration. The intensity of the TSL at both trap level decreased as $Cu^{2+}$ increases. The 75 and 240 °C trap center peaked at x = 0.025% and 0.075%, respectively and quenches thereafter.

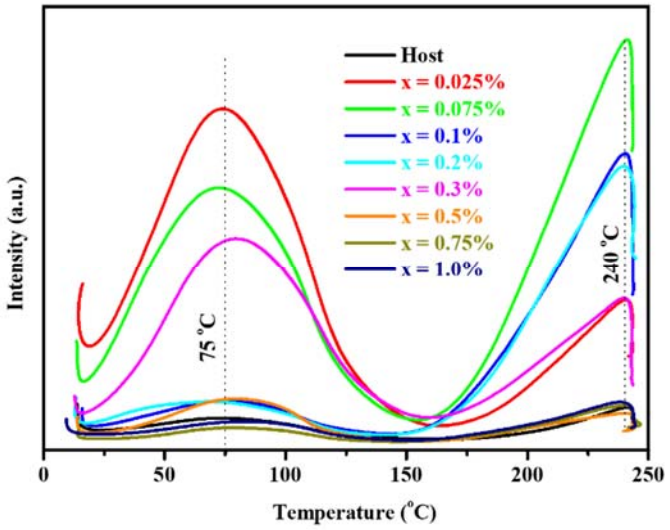


**Fig. 11.** Glow curve of the UV-irradiated $BaAl_2O_4$:x% $Cu^{2+}$ ($0 \leq x \leq 1$) nano-powder at a heating rate of 2 $°Cs^{-1}$.

## 4. Conclusion

Hexagonal $BaAl_2O_4$:x% $Cu^{2+}$ ($0 \leq x \leq 1$) nano-powders with crystallite sizes in the order of 20 nm were successfully synthesized via citrate sol-gel method. The EDS confirmed the presence of the expected elementary composition for both the host and $Cu^{2+}$ doped samples. Varying the $Cu^{2+}$ concentration changed the morphology of the prepared nano-phosphor. The TEM revealed the crystallite size and hollow tubular structures of the prepared samples. The PL results showed that there are emissions from both the intrinsic intraband gap defects and the $Cu^{2+}$ transition. The optimum $Cu^{2+}$ concentration and critical energy transfer distance (Rc) were respectively found to be 0.075% $Cu^{2+}$ and 12.01 Å. CIE colour chromaticity showed that the $Cu^{2+}$ doping excitation wavelength influence the bluish emission. TL results showed that there are both shallow and deep traps within the $BaAl_2O_4$: $Cu^{2+}$ for the investigated concentration ranges.

## Acknowledgements

This work is supported by the South African National Research Foundation (NRF) Thuthuka programme (fund number: UID 116001 and 114924). The author would like to thank Miss M.A. Ramathata for

synthesizing the phosphor materials and Dr James Wesley-Smith at Electron Microscopy Unit at Sefako Makgatho Health Science University is acknowledge for the SEM and TEM imaging.

**References**

[1] M.V.S. Rezende, P.J. Montes, M.E.G. Valerio, R.A. Jackson, Optical Materials 34 (2012) 1434.

[2] H.F. Brito, M.C.F.C. Felinto, H.T. Laamanen, M. Lastusaari, M. Malkamäki, P. Novák, L.C.V. Rodrigues, R. Stefani, Optical Materials Express 2 (4) (2012) 420.

[3] A.H. Wako, F.B Dejene, H.C Swart, Journal of Rare Earths 32 (9) (2014) 806.

[4] Q. Xie, B. Li, X. He, M. Zhang, Y. Chen, Q. Zeng, Materials 10 (2017) 1198.

[5] K.A. Gedekar, S.P. Wankhede, S.V. Moharil, R.M. Belekar, Journal of Advanced Ceramics 6 (4) (2017) 341.

[6] L.F. Koao, B.F. Dejene, H.C. Swart, Physica B: Physics of Condensed Matter 439 (2014) 173.

[7] S.V. Motloung, F.B. Dejene, L.F. Koao, O.M. Ntwaeaborwa, H.C. Swart, T.E. Motaung, O.M. Ndwandwe, Optical Materials 64 (2017) 26.

[8] V.M. Maphiri, F.B. Dejene, S.V. Motloung, Results in Physics 7 (2017) 3510.

[9] M. Zhang, C. Chen, L. Qin, K. Yan, G. Cheng, H. Jing, T. Zou, Materials Science and Technology 34 (1) (2018) 69.

[10] L.C.V. Rodrigues, J. Hölsä, J.M. Carvalho, C.C.S. Pedroso, M. Lastusaari, M.C.F.C. Felinto, S. Watanabe, H.F. Brito, Physica B 439 (2017) 67.

[11] S. Som, A.K. Kunti, V. Kumar, V. Kumar, S. Dutta, M. Chowdhury, S.K. Sharma, J.J. Terblans, H.C. Swart, Journal of Applied Physics 115 (19) (2014) 193101.

[12] G. Blasse, Journal of Solid State Chemistry 62 (1986) 207.

[13] H. Yu, J. Chen, S. Gan, Journal of Spectroscopy (2016) Article ID 9346503 1-5.

[14] http://www.mathworks.com/matlabcentral/fileexchange/29620-cie-coordinate-calculatori 2012.

[15] V. Singh, S. Watanabe, T.K. Gundu Rao, J.F.D. Chubaci, I. Ledoux-Rak, H.- Y. Kwak, Applied Physics B 98 (2010) 165.

[16] K.K. Satapathy, F. Khan, International Journal of Chemical Science and Application 3 (2012) 366.